

# Prediction of natural convection flow using network model and numerical simulations inside enclosure with distributed solid blocks

Sherifull-Din Jamalud-Din · D. Andrew S. Rees ·  
B. V. K. Reddy · Arunn Narasimhan

Received: 28 July 2009 / Accepted: 25 December 2009 / Published online: 22 January 2010  
© Springer-Verlag 2010

**Abstract** Steady state natural convection of a fluid with  $Pr \approx 1$  within a square enclosure containing uniformly distributed, conducting square solid blocks is investigated. The side walls are subjected to differential heating, while the top and bottom ones are kept adiabatic. The natural convection flow is predicted employing the nondimensional volumetric flow rate ( $Q_{\max}^*$ ) by using a network model and also using numerical simulations. For identical solid and fluid thermal conductivities (i.e.  $k_s = k_f$ ), a parametric study of the effect of number of blocks ( $N^2$ ), gap size ( $\delta$ ) and enclosure Rayleigh number ( $Ra$ ) on  $Q_{\max}^*$  is performed using the two approaches. Network model predictions are observed to agree well with that from the simulations until  $Ra\delta^3 \sim 12$ . Considering the enclosure with blocks as a porous medium, for a fixed enclosure  $Ra$  number, increasing the number of blocks for a fixed volumetric porosity leads to a decrease in enclosure permeability, which in turn reduces the flow rate. When the number of blocks is fixed, and for a given  $Ra$  number, the flow rate increases as the porosity increases by widening the gap between the blocks.

S.-D. Jamalud-Din · D. A. S. Rees  
Department of Mechanical Engineering,  
University of Bath, Claverton Down,  
Bath BA2 7AY, UK

D.A.S. Rees  
e-mail: D.A.S.Rees@bath.ac.uk

B. V. K. Reddy · A. Narasimhan (✉)  
Heat Transfer and Thermal Power Laboratory,  
Department of Mechanical Engineering,  
Indian Institute of Technology Madras,  
Chennai 600036, India  
e-mail: arunn@iitm.ac.in

B. V. K. Reddy  
e-mail: bvkreddy680@gmail.com

## List of symbols

$A$	Cross sectional area of the enclosure, $m^2$
$d$	Channel width, m
$D$	Solid block size, m
$Da$	Darcy number ( $K/L^2$ ), dimensionless
$g$	Acceleration due to gravity, $m\ s^{-2}$
$H$	Height of the cavity, m
$J$	Vector
$k$	Thermal conductivity, $W\ m^{-1}\ K^{-1}$
$K$	Permeability of the porous medium, $m^2$
$L$	Width of the cavity, m
$\dot{m}$	Mass flow rate per unit depth, $kg\ s^{-1}$
$Q^*$	Volumetric flow rate, dimensionless
$N$	Number of blocks in the first column of $N \times N$ blocks configuration
$p$	Pressure, $N\ m^{-2}$
$p^*$	Pressure, dimensionless
$Pr$	Prandtl number, $\frac{\nu}{\alpha}$
$Ra$	Rayleigh number, $\frac{g\beta(T_h - T_c)L^3}{(\alpha\nu)_f}$
$T$	Temperature, K
$u, v$	Velocity components along the $x$ and $y$ -axes, respectively, $m\ s^{-1}$
$u^*, v^*$	Velocity components along the $x$ and $y$ -axes, respectively, dimensionless
$x, y$	Coordinates, m
$x^*, y^*$	Coordinates, dimensionless

## Greek symbols

$\alpha$	Thermal diffusivity, $m^2\ s^{-1}$
$\beta$	Coefficient of thermal expansion, $K^{-1}$
$\delta$	Channel width, dimensionless
$\kappa$	Flow control parameter, dimensionless
$\phi$	Porosity of the porous medium, dimensionless
$\nu$	Kinematic viscosity, $m^2\ s^{-1}$
$\theta$	Temperature, dimensionless

$\rho$	Density, $\text{kg m}^{-3}$
$\psi$	Stream function, $\text{m}^2 \text{s}^{-1}$
$\psi^*$	Stream function, dimensionless

### Subscripts

avg	Average
c	Cold wall
f	Fluid
h	Hot wall
$i, j$	Indices corresponding to the $x$ and $y$ directions, respectively
m	Mean temperature
max	Maximum

## 1 Introduction

Natural convection flow within enclosures with obstacles approximate many real-life situations such as ventilation in grain silos [1], buildings and storage places for heat generating containers, cooling of electronic cabinets [2] and for delineating heterogeneous porous medium behavior [3]. The accurate prediction of fluid flow and heat transfer is of primary importance in the design and optimization of the above configurations. This has received recent research attention. Analyzing such convection configuration using a network model was first attempted by Oliver [4] and Koplik [5]. In [4], network model is used to predict temperature inside a transformer. By analysing the associated probability distribution function for the network, Koplik [5] calculated the total current flow across the entire network which would be the function of the voltage difference. Articles of Zhang and Li [6, 7] and Jordan [8] also provide the methodology and applications of network model theory. Apart from being used in natural convection studies, the network method has been applied recently for various engineering problems, namely, transient radiative transfer process between the thick walls of enclosures [9], simulating two-dimensional transient density-driven flow and solute transport through porous media [10], and for the simultaneous inverse determination of temperature-dependent thermophysical properties in fluids [11].

Numerical simulations have also been employed to study convection in enclosures with distributed solid blocks. House et al. [12] examined the consequence of placing a centered, square, heat-conducting body in a square enclosure. This work was extended in the parametric range  $10^3 < Ra < 10^6$  and  $0.1 < Pr < 10$ , by Bhave et al. [13] and an optimum heat transfer enhancement was deduced by controlling both the size and thermal conductivity of the solid block. Natural convection in an enclosure with multiple blocks was first investigated by Merrikh and Mohamad [14]. The intrusion of blocks within the side-wall thermal

boundary layers was reported to inhibit convection. In [15], block distribution effect on the overall enclosure convection was studied, while in [3], effect of uniformly placed conducting solid objects was studied using a continuum model. For a given Rayleigh number, strong hindrance effect of the blocks on the convection process was reported beyond a minimum number of blocks.

In [16], steady laminar and turbulent natural convection within a cavity with solid conducting blocks were investigated. Their conclusion that the macroscopic model did not predict the average Nusselt number well, when compared with those obtained from the continuum model with several obstacles, was also reported by Massarotti et al. [17]. In [18], natural convection in enclosure with a random distribution of solid blocks was studied. An oscillatory behaviour was observed in the local wall Nusselt number and a critical Rayleigh number for the onset of convection was also predicted.

The objective in this study is to predict the natural convection flow rate inside a square enclosure distributed with solid blocks using the network model and compare it with corresponding predictions from equivalent numerical simulations. The comparison provides bounds for the applicability of the developed network model in predicting such enclosure convection flow rate, a contribution unavailable at present in the published literature. For completion, a parametric study, using porous medium approach, is also performed.

## 2 Geometry and problem formulation

The system being investigated is shown in the two dimensional schematic in Fig. 1. It consists of a fluid-saturated square enclosure containing several conducting square solid obstacles. They are disconnected and distributed uniformly within the enclosure, which is itself subjected to a horizontal temperature difference ( $\Delta T = T_H - T_C$ ) applied at the walls as shown in Fig. 1. The resulting natural convection of the fluid due to buoyancy effects results in a flow within the enclosure through the gaps between the solid blocks.

The flow is governed by the two-dimensional version of the three conservation equations: mass, momentum (Navier–Stokes) and the heat transport equations subject to various assumptions. The Boussinesq approximation, where the local density varies only with temperature and only within the buoyancy term, has been invoked. Further, the Newtonian fluid is assumed to remain in a single phase state with constant thermal and physical properties. The resulting laminar incompressible flow is then in steady state natural convection. The governing equations for mass, momentum in the  $x$  and  $y$  directions and heat transport are as follows:

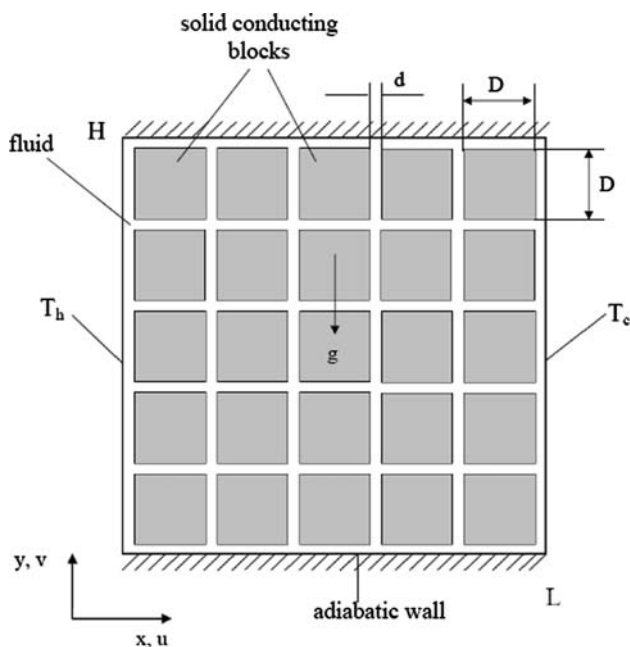


Fig. 1 Schematic of enclosure configuration with 5 × 5 block array

$$\frac{\partial u}{\partial x} + \frac{\partial v}{\partial y} = 0 \tag{1}$$

$$\left( u \frac{\partial u}{\partial x} + v \frac{\partial u}{\partial y} \right) = -\frac{1}{\rho} \frac{\partial p}{\partial x} + \nu \left( \frac{\partial^2 u}{\partial x^2} + \frac{\partial^2 u}{\partial y^2} \right) \tag{2}$$

$$\left( u \frac{\partial v}{\partial x} + v \frac{\partial v}{\partial y} \right) = -\frac{1}{\rho} \frac{\partial p}{\partial y} + \nu \left( \frac{\partial^2 v}{\partial x^2} + \frac{\partial^2 v}{\partial y^2} \right) + g\beta(T - T_m) \tag{3}$$

$$\rho c_p \left( u \frac{\partial T}{\partial x} + v \frac{\partial T}{\partial y} \right) = k \left( \frac{\partial^2 T}{\partial x^2} + \frac{\partial^2 T}{\partial y^2} \right) \tag{4}$$

Inside the conducting solid blocks, the heat transport equation, Eq. 4, is solved by setting  $k = k_s$  and both the velocity components to zero.

The governing equations Eqs. 1–4 are nondimensionalized using the following variables

$$x^* = \frac{x}{L}, \quad y^* = \frac{y}{L}, \quad u^* = \frac{uL}{\alpha_f}, \quad v^* = \frac{vL}{\alpha_f}, \quad p^* = \frac{\rho L^2}{\rho(\alpha\nu)_f} \tag{5}$$

$$\theta = \frac{T - T_c}{T_h - T_c}, \quad Ra = \frac{g\beta(T_h - T_c)L^3}{(\alpha\nu)_f} \tag{5}$$

leading to the nondimensionalized forms of Eqs. 1–4, written as

$$\frac{\partial u^*}{\partial x^*} + \frac{\partial v^*}{\partial y^*} = 0 \tag{6}$$

$$\frac{1}{Pr} \left( u^* \frac{\partial u^*}{\partial x^*} + v^* \frac{\partial u^*}{\partial y^*} \right) = -\frac{\partial p^*}{\partial x^*} + \left( \frac{\partial^2 u^*}{\partial x^{*2}} + \frac{\partial^2 u^*}{\partial y^{*2}} \right) \tag{7}$$

$$\frac{1}{Pr} \left( u^* \frac{\partial v^*}{\partial x^*} + v^* \frac{\partial v^*}{\partial y^*} \right) = -\frac{\partial p^*}{\partial y^*} + \left( \frac{\partial^2 v^*}{\partial x^{*2}} + \frac{\partial^2 v^*}{\partial y^{*2}} \right) + Ra \left( \theta - \frac{1}{2} \right) \tag{8}$$

$$\left( u^* \frac{\partial \theta}{\partial x^*} + v^* \frac{\partial \theta}{\partial y^*} \right) = \left( \frac{\partial^2 \theta}{\partial x^{*2}} + \frac{\partial^2 \theta}{\partial y^{*2}} \right) \tag{9}$$

The associated boundary conditions for Eqs. 6–9 with respect to the geometry shown in Fig. 1 are

At the left hot wall

$$x^* = 0: \quad u^* = v^* = 0, \quad \theta = 1. \tag{10}$$

At cold wall

$$x^* = 1: \quad u^* = v^* = 0, \quad \theta = 0. \tag{11}$$

And at the upper and lower walls

$$y^* = 0, 1: \quad u^* = v^* = 0, \quad \frac{\partial \theta}{\partial y^*} = 0. \tag{12}$$

Velocity boundary conditions similar to the above Eqs. 10–12 are applied to the corresponding vertical and horizontal walls of the conducting solid blocks along with the following continuity of temperature and heat flux conditions,

$$\theta_f = \theta_s, \quad k_f \left( \frac{\partial \theta_f}{\partial n} \right) = k_s \left( \frac{\partial \theta_s}{\partial n} \right), \tag{13}$$

where  $n$  denotes the direction normal to the corresponding wall of each block.

### 3 Solution methodology

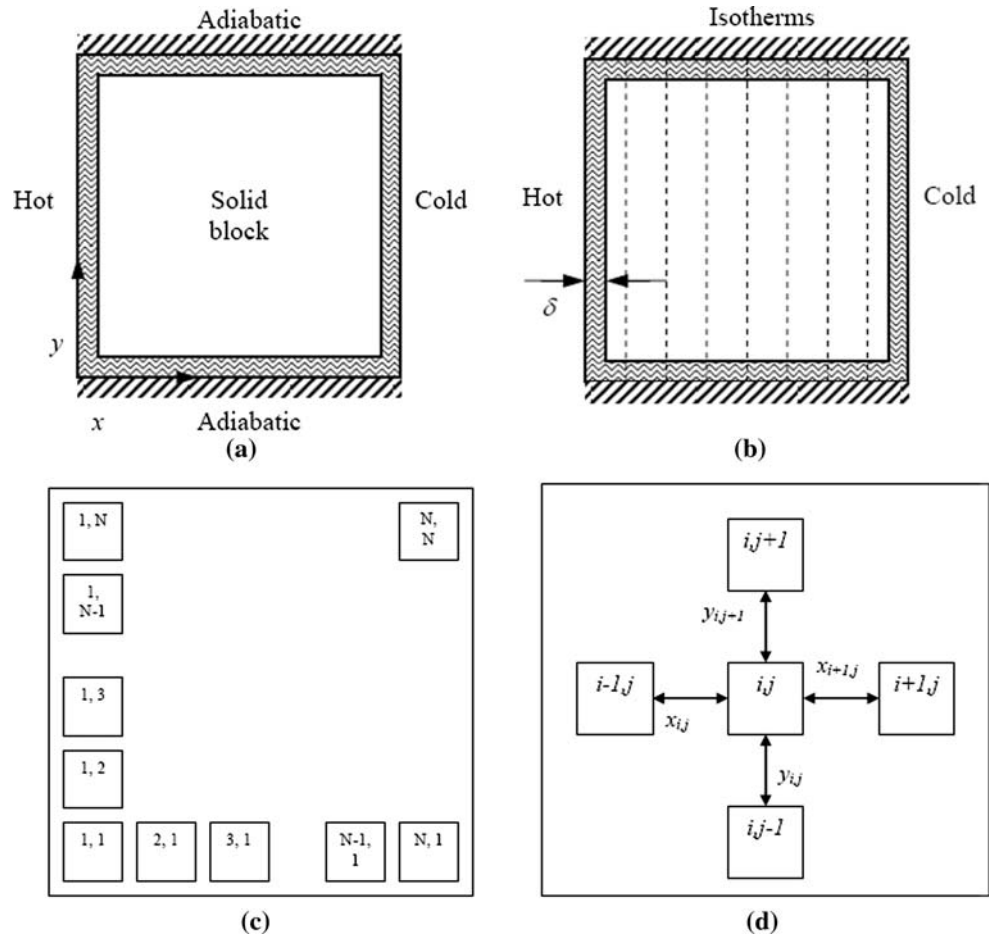
The governing equations Eqs. 6–9 are solved together with associated boundary conditions Eqs. 10–13 by means of two approaches, namely, an analytical network model [19] and the primary-variable-based numerical simulation [20]. The two approaches are explained as follows.

#### 3.1 Network model theory

The schematic in Fig. 1 is one instance of a more generic case of an enclosure with blocks as depicted in Fig. 2. This would prompt one in the first instance to study the natural convective flow in an enclosure saturated with a fluid, bathing a single conducting block as shown in Fig. 2a, before generalizing the analysis to enclosure containing larger numbers of blocks (Fig. 2c).

On substituting the relations  $u^* = \partial\psi^*/\partial y^*$  and  $v^* = \partial\psi^*/\partial x^*$  into Eqs. 7 and 8 one obtains the equivalent stream function formulation. This enables the plotting of streamlines—lines that are, at given instant, tangent to the

**Fig. 2** **a** Single block configuration, **b** Isotherms, **c** Multiple block configuration, **d** Block  $(i, j)$  and its neighbouring blocks and gaps



direction of flow at every point in the flow field. These equations are then cross differentiated with respect to  $y^*$  and  $x^*$  and the resulting equations are subtracted from one another to eliminate the pressure term, resulting in a single momentum equation of the form,

$$\frac{\partial \psi^*}{\partial x^*} \nabla^2 \left( \frac{\partial \psi^*}{\partial y^*} \right) - \frac{\partial \psi^*}{\partial y^*} \nabla^2 \left( \frac{\partial \psi^*}{\partial x^*} \right) = \nabla^4 \psi^* + \frac{\partial \theta}{\partial x^*} Ra \quad (14)$$

Equation 14 may only be solved if the temperature profile  $(\theta)$ , is known. For the network model, it will be assumed the flow within the gaps is sufficiently weak that the isotherms remain vertical, at least to leading order in  $\delta$ , where  $\delta$  is the gap width; this is depicted in Fig. 2b. Therefore the temperature field is taken to be,

$$\theta = 1 - x^* \quad (15)$$

A further assumption that is made is that the flow in all the channels shown in Figs. 1, 2a is unidirectional. The possible errors incurred due to entrance and corner effects are neglected. Observe that, by imposing these assumptions for flow and temperature as in Eq. 15, one doesn't preclude the overall two dimensionality of the flow through the channels in the enclosure shown in Fig. 1. After substitution of Eq. 15, Eq. 14 becomes,

$$\frac{\partial \psi^*}{\partial x^*} \nabla^2 \left( \frac{\partial \psi^*}{\partial y^*} \right) - \frac{\partial \psi^*}{\partial y^*} \nabla^2 \left( \frac{\partial \psi^*}{\partial x^*} \right) = \nabla^4 \psi^* - Ra \quad (16)$$

The solution procedure for the flow in the channels for both the single block and multiple block cases is given in detail in [19]. To summarise briefly, within each channel it is possible to find the detailed flow, which is a combination of plane Poiseuille flow and buoyancy-induced channel flow. Thus it is possible to relate the overall mass flow within each channel to the uniform pressure gradient along the channel. In turn, this leads to an equation relating the pressure drop along the channel to difference between the values of the stream function across the channel. The pressure change when moving around any one chosen block must be zero, and therefore this becomes equivalent to an equation relating the value of  $\psi$  stream function (dimensional) on the chosen block to the corresponding values of its four neighbours.

The maximum mass flow rate circulating within the cavity (e.g. from the heated wall to the centre of the enclosure) can be written as

$$\dot{m} = \rho \times A \times \frac{1}{L} \int_0^{L/2} u dy \quad (17)$$

where  $\dot{m}$  is mass flow rate per unit depth and  $A(=L/2 \times 1)$  is the cross sectional area of the enclosure from the heated wall to the centre.

Using the above  $\dot{m}$  definition in Eq. 17, a non-dimensional volumetric flow rate can be written in the form,

$$Q^* = \frac{\dot{m}}{(\rho\alpha)_f} = \int_0^{1/2} u^* dy^* = \int_0^{1/2} \frac{\partial\psi^*}{\partial y^*} dy^* \tag{18}$$

By following the procedure described above, it is possible to determine the stream function corresponding to each of the blocks within the cavity, and hence it is possible to determine the volumetric flow rate in each channel. For the single block case, as shown in Fig. 2a, we obtain,

$$Q^* = \int_0^{1/2} u^* dy^* = \frac{1}{48} Ra \delta^3 \tag{19}$$

For multiple block situations the stream function at block  $(i, j)$  (see Fig. 2d) is given in terms of its four neighbours:

$$4Q_{ij}^* - Q_{i-1,j}^* - Q_{i+1,j}^* - Q_{i,j-1}^* - Q_{i,j+1}^* = \frac{2}{3} \left(\frac{\delta}{2}\right)^3 Ra \tag{20}$$

Equation 20 is applied over  $N \times N$  blocks, and the resulting simultaneous equations can be expressed in matrix/vector form where the matrix contains  $N^2 \times N^2$  elements. This may be written in the form

$$M_{N^2 \times N^2} \times \underline{Q}_{N^2}^* = \kappa \times J_{N^2} \tag{21}$$

where  $M$  is a block tri-diagonal matrix,  $\underline{Q}^*$  is the vector of values of the stream function on each block and  $J$  is a vector of length  $N^2$  consisting entirely of ones. The parameter  $\kappa$  controls the flow and is defined as

$$\kappa = \frac{2}{3} \left(\frac{\delta}{2}\right)^3 Ra \tag{22}$$

**Table 1** Grid independence study for  $N = 10$  and  $20$  with uniformly spaced blocks with  $\delta = 0.005, L^* = 1$  using  $Ra\delta^3 = 1.2$

Grid size	$Q_{avg}^*$	$Q_{max}^*$	Percentage error in the maximum volumetric flow rate $\frac{ Q_{new}^* - Q_{old}^* }{Q_{new}^*} \times 100$
$N = 10, Q_{max}^* = 0.0873$ (Network model theory)			
160 × 160	0.0474	0.0894	
300 × 300	0.0461	0.0915	2.295
600 × 600	0.0453	0.0907	0.820
1,200 × 1,200	0.0448	0.0900	0.778
$N = 20, Q_{max}^* = 0.1615$ (Network model theory)			
200 × 200	0.0778	0.5415	
300 × 300	0.0889	0.1690	220.41
520 × 520	0.0863	0.1727	2.14
1,440 × 1,440	0.0847	0.1697	1.77

Thus, from Eq. 21 the values of the volumetric flow rate array  $Q_{N^2}^*$  can be calculated using standard matrix inversion method like Gauss Siedel iterative procedure.

### 3.2 Direct simulations using primary variables

For validating the above network model results, a separate primary variables based numerical simulation of the enclosure with corresponding number of blocks was also performed. The numerical simulations are performed using the finite volume formulation of Eqs. 6–9 together with the associated boundary conditions given in Eqs. 10–13. The convective terms of Eqs. 6–9 are discretized using a power law scheme and the diffusion terms with the central difference scheme. The pressure and velocity coupling are performed by using the SIMPLE algorithm [20], and are solved iteratively using the tri-diagonal matrix algorithm.

Suitable grids were chosen after performing grid independence tests of the steady state results for all the number of blocks and gap sizes considered. The convergence criteria for the mass, momentum and energy equations were set as  $10^{-5}, 10^{-5}$  and  $10^{-13}$  respectively. Owing to space constraints, representative grid independence results for the  $N = 10$  and  $20$  with size,  $\delta = 0.005$ , are reported in Table 1. Based on these results, a grid of size (the number of grid points in solid block is approximately five times that in fluid within the gaps)  $1200 \times 1200$  was used for  $N = 10$  and, for the  $N = 20$  case, a  $1440 \times 1440$  grid was taken. For other cases with larger number of blocks, the grid sizes were meticulously chosen by performing similar grid independence tests.

## 4 Results and discussion

Using the two approaches detailed in the previous section, the effect of number of blocks ( $N^2$ ), channel width ( $\delta$ ) and

Rayleigh number ( $Ra$ ) on the maximum volumetric flow rate ( $Q_{\max}^*$ ) are studied in detail.

For an enclosure of unit aspect ratio (i.e.  $H = L$  in Fig. 1), once the volumetric porosity  $\phi$  of the enclosure and the number of solid blocks  $N^2$  placed within it are known, the block size ( $D^*$ ) and the channel width ( $\delta$ ) can be determined uniquely using the relations,

$$\phi = 1 - N^2 D^{*2} \quad (23)$$

and

$$\delta = \frac{1 - D^* N}{N + 1}, \quad (24)$$

where the latter is obtained by observing that a cavity wall has the same length as  $N + 1$  channel widths and  $N$  blocks.

The present enclosure with conducting blocks may be treated as an equivalent porous enclosure without losing the generality of the results. This equivalent porous medium allows one to calculate the permeability,  $K$ , using the Carman-Kozeny relationship [2, 21]. Here,  $K$  will be a function of the enclosure volumetric porosity, the number of blocks (porous medium particle length scale) and the gap width (pore length scale). The non-dimensional version of this relationship may be written as

$$Da = \frac{K}{L^2} = \frac{1}{180} \frac{\phi^3 D^{*2}}{(1 - \phi)^2} \quad (25)$$

where  $Da$ , Darcy number, is the non-dimensional representation of the permeability of the block-filled enclosure when treated as a porous medium.

In the numerical simulations for the enclosure with conducting blocks, the enclosure volumetric porosity  $\phi$  is kept fixed at 0.2 and the  $N^2$  is changed from 25 to 400, with the corresponding reduction in the block size ( $D^*$ ). The streamlines and the isotherms are shown in Figs. 3, 4 and 5 for several combinations of values of  $Ra\delta^3$  and  $N^2$ . The blocks are shown as dotted lines in these Figures. It is important to note that, when these configurations are treated as a porous medium, their corresponding permeabilities decrease as the number of blocks increases, as deduced from Eq. 25. The corresponding  $Da$  values, as calculated from Eq. 25, are given in the respective figure captions.

For a chosen enclosure configuration, with a fixed number of blocks as shown in Fig. 3 and a fixed gap width, the isotherms bend increasingly from (a) to (c), indicating that convection effects are becoming progressively stronger as  $Ra$  is increased. This effect is also observed when the number of blocks is increased from 5 to 10 and 20, as shown in Figs. 4, 5. However, in general, increasing the number of blocks for a fixed volumetric porosity leads to decrease in effective permeability of the cavity and causes reduction in flow rate. Hence, the temperature gradients near the hot wall will become lower. This, in turn, results in

lesser heat transfer. Indeed, while the Rayleigh number remains fixed for these three cases, a porous-Rayleigh number based upon  $KL$  (instead of  $L^3$  for the pure fluid Rayleigh number) decreases as the number of blocks increases for a fixed porosity.

For  $Pr \approx 1$  and  $k_s = k_f$ , the maximum volumetric flow rate ( $Q_{\max}^*$ ) for the above configurations have been calculated using the two methods (network model and simulations), and are plotted in Fig. 6 as a function of  $Ra\delta^3$  and number of blocks ( $N^2$ ). The results are seen to be in good agreement. However, it is important to note that the results of the network model are independent of  $Pr$  and  $k_s/k_f$ . When the enclosure permeability is the least ( $N^2 = 400$  case), the isotherms as observed in Fig. 5, remain roughly linear, irrespective of the Rayleigh number. The isotherms in Fig. 3 deviate greatly from the assumption in Eq. 15 explaining the fairly large difference between the results from the two methods in Fig. 6 when  $N^2 = 25$ .

If one were to consider a fixed value of  $Ra\delta^3$  in Fig. 6, then one may observe that  $Q_{\max}^*$  increases as the number of blocks increases from  $N^2 = 25$  to  $N^2 = 400$ . This appears to be counter-intuitive as one would expect the flow rate to decrease as an increasing number of blocks at a fixed porosity necessarily results in a decrease in the channel widths. On treating the configuration as a porous media, this translates to a decrease in permeability as indicated in Fig. 6, which is also expected to decrease the flow rate. However, in this situation, the effects of  $Ra$  and gap size ( $\delta$ ) are not mutually exclusive. For a fixed value of  $Ra\delta^3$  on the abscissa, an increasing number of blocks decreases the gap size, but it also increases the value of the Rayleigh number since  $Ra\delta^3$  is held constant. This results in stronger convection as one proceeds from  $N^2 = 25$  to  $N^2 = 400$  blocks, which, in turn, results in the higher flow rate observed in the Fig. 6 results.

To corroborate the validity of this reasoning, a decreased permeability can be shown to decrease the flow rate within the enclosure. This result can be obtained from the results in Fig. 6 itself in the following way. For a constant porosity  $\phi = 0.2$ , for  $N^2 = 25$  one could predict the flow rate from the ordinate of Fig. 6 when, say,  $Ra\delta^3 = 12$ , as marked by point A in the Figure. Given that  $N^2 = 25$  at point A and that the gap width is known, one could obtain a Rayleigh number from the equation  $Ra\delta^3 = 12$ . For this same Rayleigh number, in the  $N^2 = 100$  case, the corresponding flow rate is smaller, as marked by point B, since the permeability is reduced as the gap size is reduced. A similar argument leads to an even weaker flow rate for the same value of the Rayleigh number, when the number of the blocks increases to  $N^2 = 400$  as marked by point C. This effect is captured well by both the network model and the numerical simulations.

**Fig. 3** Streamlines and isotherms for enclosure with  $N = 5$ ,  $\phi = 0.2$  and  $Da = 0.22 \times 10^{-6}$  at  $Ra\delta^3 =$  (a) 0.12, (b) 1.2, (c) 12

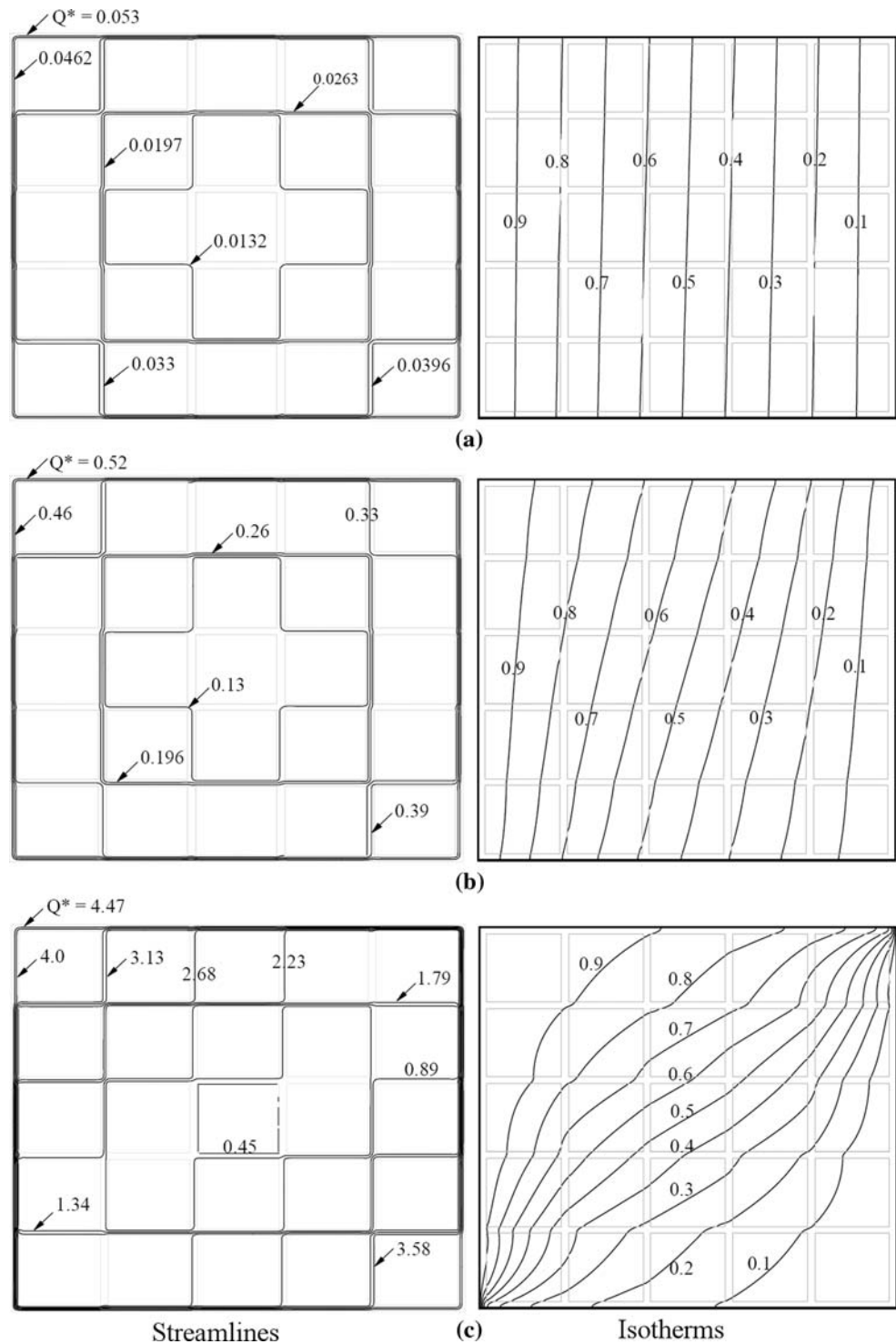
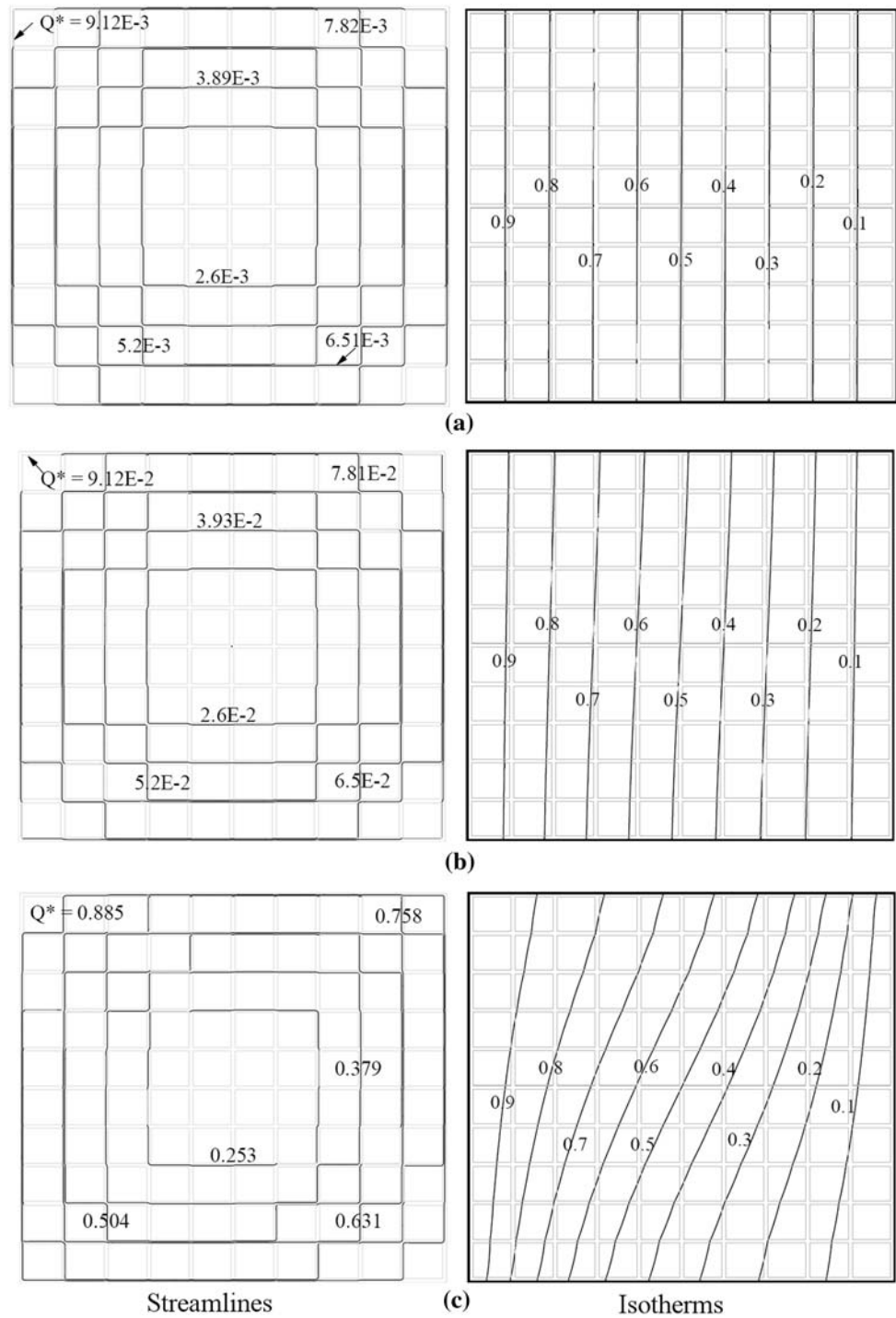


Figure 7 depicts the variation of maximum volumetric flow rate  $Q_{\max}^*$  with Rayleigh number for three different porosities while retaining a fixed number of blocks at  $N^2 = 100$ . It is to be expected that convection is enhanced when  $Ra$  is increased for a fixed value of  $\delta$  and it is also enhanced as the gap width,  $\delta$ , increases for a fixed Rayleigh

number. In the latter case the effective permeability increases, which must lead to stronger flows. Both the network model and numerical simulations agree well in the prediction of these results.

These observations can be summarized in a plot as done in Fig. 8 subsuming the permeability variation in  $RaDa$ ,

**Fig. 4** Streamlines and isotherms for enclosure with  $N = 10$ ,  $\phi = 0.2$  and  $Da = 5.56 \times 10^{-7}$  at  $Ra\delta^3 =$  (a) 0.12, (b), 1.2 (c) 12

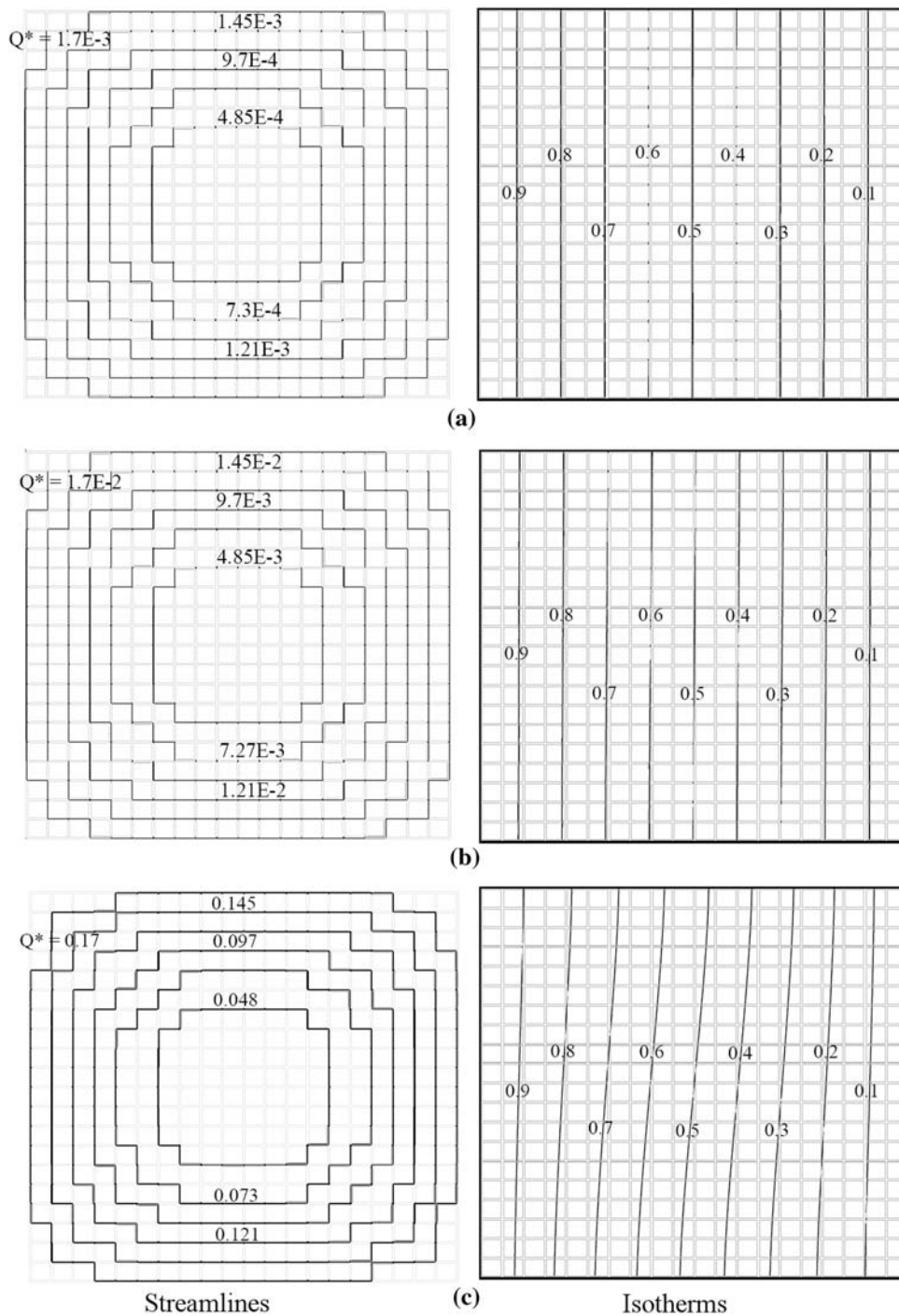


the conventional KL length scale based porous medium Rayleigh number. This plot reduces effectively the flow rate information for several enclosure with obstacles configurations into a succinct porous medium range, exploiting the use of treating enclosures with obstacles as a porous medium.

## 5 Conclusions

Steady natural convection inside a side wall heated square enclosure filled with uniformly distributed conducting solid blocks has been investigated using two approaches. Results from network model theory were compared with numerical

**Fig. 5** Streamlines and isotherms for enclosure with  $N = 20$ ,  $\phi = 0.2$  and  $Da = 1.39 \times 10^{-7}$  at  $Ra\delta^3 =$  (a) 0.12, (b) 1.2, (c) 12



simulation results using primary variables. For the considered range of parameters, the network model predictions of enclosure flow rate ( $Q_{max}^*$ ) agree well with the numerical simulations until  $Ra\delta^3 \sim 12$ .

For a fixed porosity ( $\phi$ ), both the network model and the simulations predict an increase in the maximum volumetric enclosure flow rate when the number of blocks is increased. This counter-intuitive result is because of the

constancy of the  $Ra\delta^3$  group. This leads to stronger convection due to increase in  $Ra$  number, when the gap size decreases (due to increase in the number of blocks  $N$ ). For identical  $Ra$  numbers, the maximum volumetric flow rate decreases, as expected, when the number of blocks is increased.

Treating the enclosure with blocks as a porous medium, for a fixed  $Ra$ , an increase in the number of blocks for a fixed

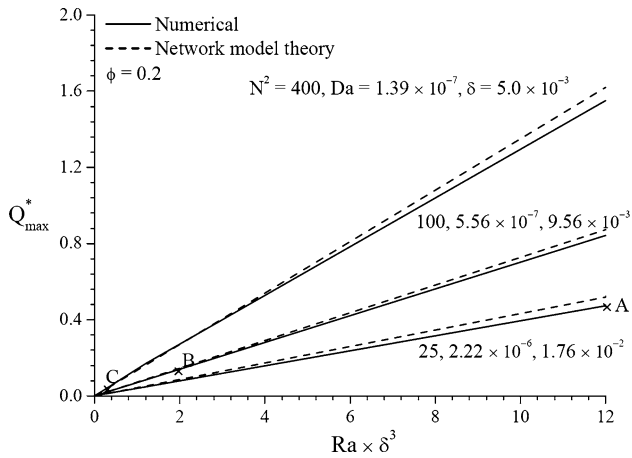


**Fig. 6** Variation of  $Q_{\max}^*$  with number of blocks ( $N^2$ ) for fixed porosity  $\phi = 0.2$

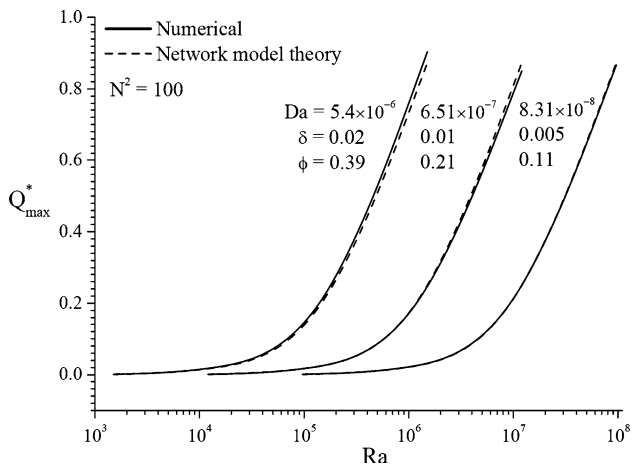


**Fig. 7** Variation of  $Q_{\max}^*$  with porosity for number of blocks  $N^2 = 100$

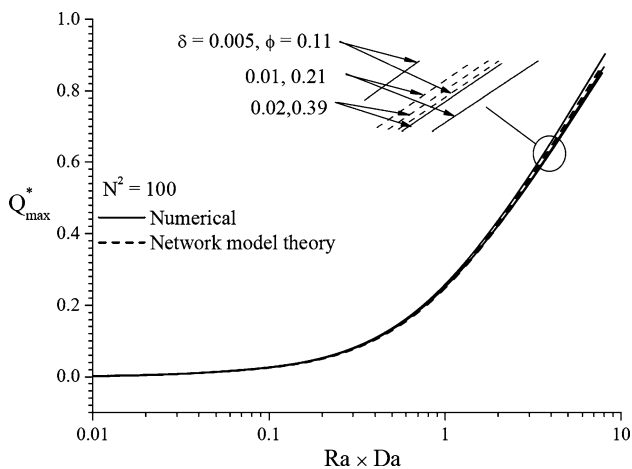


**Fig. 8** Variation of  $Q_{\max}^*$  with  $Ra Da$  for number of blocks  $N^2 = 100$

porosity leads to a decrease in the enclosure permeability ( $Da$ ), reducing the flow rate. For a configuration with fixed number of blocks, increasing the porosity by increasing the gap size, increases the flow rate for a given  $Ra$ .

Using conventional porous medium  $Ra$  number ( $=RaDa$ ) the flow rate information for several enclosure with obstacles configuration is shown to be reduced into a few equivalent porous medium configuration. This result highlights the engineering use of treating such enclosure configurations as a porous medium.

**References**

1. Fohr J, Moussa HB (1994) Heat and mass transfer in a cylindrical grain silo submitted to a periodical wall heat flux. *Int J Heat Mass Transf* 37(12):1699–1712
2. Nield DA, Bejan A (2006) *Convection in Porous Media*, 3rd edn. Springer, New York
3. Merrikh AA, Lage JL (2005) Natural convection in an enclosure with disconnected and conducting solid blocks. *Int J Heat Mass Transf* 48(7):1361–1372
4. Oliver AJ (1980) Estimation of transformer winding temperatures and coolant flows using a general network method. *Proc Int Elect Engg C* 127:395–405
5. Koplik J (1981) On the effective medium theory of random linear networks. *J Phys C Solid State Phys* 14:4821–4837
6. Zhang J, Li X (2002) A comprehensive resistance network-based hydraulic model for coolant flow in disk-type electrical transformer windings. In: Dost S, Struchtrup H, Dincer I (eds) *Progress transport phenomena: proceedings of the 13th international symposium on transport phenomena*, New York, pp 545–550
7. Zhang J, Li X (2006) Oil cooling for disk-type transformer windings, Part 1: theory and model development. *IEEE Trans Pow Deliv* 21(3):1318–1325
8. Jordán JZ (2006) Network method to study the transient heat transfer problem in a vertical channel with viscous dissipation. *Int Commun Heat Mass Transf* 33(9):1079–1087
9. Zueco J, Campo A (2006) Network model for the numerical simulation of transient radiative transfer process between the thick walls of enclosures. *Appl Therm Eng* 26:673–679
10. Meca AS, López FA, Fernández CG (2007) Density-driven flow and solute transport problems: a 2-D numerical model based on the network simulation method. *Comput Phys Commun* 177:720–728
11. Zueco J, Alhama F (2007) Simultaneous inverse determination of temperature-dependent thermophysical properties in fluids using the network simulation method. *Int J Heat Mass Transf* 50:3234–3243
12. House JM, Beckermann C, Smith TF (1990) Effect of a centered conducting body on natural convection heat transfer in an enclosure. *Numer Heat Transf A* 18:213–225
13. Bhave P, Narasimhan A, Rees DAS (2006) Natural convection heat transfer enhancement using adiabatic block: optimal block size and Prandtl number effect. *Int J Heat Mass Transf* 49:3807–3818
14. Merrikh AA, Mohamad AA (2001) Blockage effects in natural convection in differentially heated enclosures. *J Enhanc Heat Transf* 8(1):55–72
15. Merrikh AA, Lage JL (2004) Effect of distributing a fixed amount of solid constituent inside a porous medium enclosure on the heat transfer process. *Proc Int Conf Appl Porous Media*, pp 51–57
16. Braga EJ, de Lemos MJS (2005) Heat transfer in enclosures having a fixed amount of solid material simulated with

- heterogeneous and homogeneous models. *Int J Heat Mass Transf* 48:4748–4765
17. Massarotti N, Nithiarasu P, Carotenuto A (2003) Microscopic and macroscopic approach for natural convection in enclosures filled with fluid saturated porous medium. *Int J Numer Methods Heat Fluid Flow* 13(7):862–886
  18. Pourshaghagh V, Hakkaki-Fard A, Mahdavi-Nejad A (2007) Direct simulation of natural convection in square porous enclosure. *Energy Convers Manage* 48:1579–1589
  19. Jamalud-Din S (2007) Convective flow in a square cavity filled with solid conducting blocks. Dissertation, University of Bath
  20. Patankar S (1980) Numerical heat transfer and fluid flow. Taylor and Francis
  21. Kozeny M (1927) Über kapillare Leitung des Wassers im Boden. *Sitzber Akad Wiss Wein, Math-naturw* 136:Abt IIA, p 277